Earthquake Geotechnical Engineering for Protection and Development of Environment and Constructions – Silvestri & Moraci (Eds)
© 2019 Associazione Geotecnica Italiana, Rome, Italy, ISBN 978-0-367-14328-2

Full waveform inversion to evaluate liquefaction triggering in soils exhibiting natural spatial stiffness variability

J.T. Coe, S. Mahvelati & A. Kordjazi
Temple University, Philadelphia, Pennsylvania, USA

ABSTRACT: Liquefaction triggering procedures based on the standard penetration test (SPT) and cone penetration test (CPT) each have seen a significant history of development. More recently, liquefaction triggering methodologies based on shear wave velocity (V_S) from geophysical measurements have been developed. Typically, estimates for V_S in these procedures have been acquired using downhole geophysical methods. SPT, CPT, and downhole geophysical techniques are point sources of information that only provide data in the localized region surrounding the measurement location. Therefore, these methods may not provide sufficient information regarding liquefaction triggering in soils that exhibit appreciable natural spatial variability with respect to stiffness. Surface wave methods can cover a larger spatial area and address this concern. However, surface wave methods suffer from uncertainty and spatial averaging due to the wavefield transformations used to evaluate dispersion characteristics of the underlying soils and the inherent one-dimensional assumption built into typical inversion algorithms. This study numerically modeled the propagation of surface waves in a spatially correlated Gaussian random field to simulate the effects of natural soil variability on data acquired using the multichannel analysis of surface waves (MASW). The goal was to study the capabilities of a full waveform inversion (FWI) approach when used to evaluate liquefaction triggering in spatially variable soil conditions. The results demonstrated that a FWI approach outperforms the typical dispersion-based MASW approach when implementing V_S-based liquefaction triggering procedures in spatially variable soil conditions.

1 INTRODUCTION

1.1 *Liquefaction*

Liquefaction of loose, cohesionless, saturated soils continues to be a major geotechnical issue as highlighted in recent notable seismic events such as the 2010 Mw 7.0 Darfield, 2011 Mw 6.2 Christchurch, and 2015 Mw 7.8 Gorkha earthquakes. The strength loss and post-liquefaction settlements from excess pore pressure dissipation can cause significant ground deformation. Given the devastating effects of liquefaction, a significant amount of research has explored a wide range of issues, including susceptibility (Chung & Rogers 2017), effects on infrastructure (Turner et al. 2016), and mitigation or ground improvement (Ben Salem et al. 2017).

The first step to evaluate liquefaction risk involves determining whether liquefaction triggers at a site based on anticipated seismic accelerations. Considerable efforts have been made to evaluate liquefaction triggering (e.g., Seed & Idriss 1971, Seed et al. 1985, Robertson & Wride 1998, Boulanger & Idriss 2014). These efforts have centered on a simplified stress-based approach that compares the liquefaction resistance [i.e., cyclic resistance ratio (*CRR*)] of a soil to the shear loading imparted by vertically propagating shear waves [i.e., cyclic stress ratio (*CSR*)]:

$$FS = \frac{CRR}{CSR} \tag{1}$$

$$CSR_{M=7.5}(z) = CSR_{M=m}(z) \cdot \frac{1}{MSF} = 0.65 \cdot \frac{\tau_{c,max}(z)}{\sigma'_{vo}} \cdot \frac{1}{MSF} = 0.65 \cdot \frac{(PGA/g) \cdot \sigma_{vo}(z) \cdot r_d}{\sigma'_{vo}} \cdot \frac{1}{MSF} \quad (2)$$

where FS is the factor of safety against liquefaction triggering, z is the depth, $\tau_{c,max}$ is the maximum cyclic shear stress at z, σ'_{vo} is the initial vertical effective stress, σ_{vo} is the initial vertical total stress, PGA is the peak horizontal ground acceleration, g is the acceleration due to gravity, r_d is a depth-dependent shear stress reduction coefficient, and MSF is a magnitude scaling factor that adjusts CSR for a reference earthquake magnitude M = 7.5. NASEM (2016) provides an excellent summary of these factors and this approach.

The CRR of a soil is defined as the CSR that is expected to initiate liquefaction. CRR is quantified from site characterization of geotechnical conditions, including water table location, soil stiffness, fines content, and soil fabric and stress history. The most common in situ parameters used to quantify CRR include the corrected blow count [$(N_1)_{60}$] from SPT, the corrected tip resistance (q_{c1N}) from CPT, and shear wave velocity (V_S) acquired from small-strain geophysical testing (e.g., Robertson & Wride 1998, Andrus & Stokoe 2000, Boulanger & Idriss 2014). A significant amount of research has been performed to calibrate CRR from case histories of liquefaction (e.g., see NASEM 2016).

1.2 *Spatial variability and liquefaction*

One aspect of liquefaction that has increasingly received attention is the effect of natural spatial variability. All geologic deposits exhibit variability that can be quite complex and attributable to disparate sources of uncertainty (e.g., inherent soil variability, data scatter, measurement errors, etc.) (Phoon & Kulhawy 1999). Since CRR is based on measurements of in situ soil parameters, the inherent variability present in natural deposits can influence the potential for liquefaction triggering. Most estimates of CRR in practice are obtained from SPT and CPT measurements. The point-source nature of these measurements may therefore obscure important trends in the extent of liquefaction triggering throughout a site.

A number of recent efforts have explored the effects of spatial variability on liquefaction. In many cases, a numerical probabilistic framework was explored (e.g., Popescu et al. 2005, Baker & Faber 2008, Montgomery & Boulanger 2016). However, Bong & Stuedlein (2018) recently used field data to estimate random field model (RFM) parameters for CPT tip resistance correction factors as applied to examine spatial variability of liquefaction-induced differential settlements. However, absent in the literature is discussion of how spatial variability can affect V_S measurements used to estimate CRR.

1.3 *Geophysical measurements of shear wave velocity*

Small-strain shear stiffness, as quantified via V_S, can be used to estimate CRR (e.g., Andrus & Stokoe 2000). This approach has the advantage of directly measuring a fundamental property of the soil and not a penetration resistance. Measurements of V_S are also less affected by the presence of fines. Therefore, there is less need to correct the V_S to a "clean sand" reference value as is common with penetration resistances.

Geophysical measurements of V_S have traditionally relied on instrumented boreholes (e.g., cross hole seismic method, suspension logging) or penetrometers (e.g., downhole seismic CPT). The high costs associated with these approaches have typically limited the use of V_S for liquefaction triggering analysis (Kayen et al. 2013). However, the increase in popularity of surface wave methods such as the spectral analysis of surface waves (SASW) and multichannel analysis of surface waves (MASW) methods has decreased the reliance on borehole geophysics to estimate V_S. Both SASW and MASW rely on measurements of surface waves from receivers located at the ground surface. The raw data is processed to generate a dispersion curve that represents the site-specific frequency-dependency of the surface waves. An inversion process then matches the field dispersion curve to theoretical curves from forward modeling. When the misfit is

minimized between the field and theoretical dispersion curves, the forward model is assumed to represent true field conditions. The noninvasive nature of SASW and MASW allows rapid estimates of V_S and has encouraged the use of liquefaction triggering V_S-*CRR* relationships.

Geophysical measurements can play a key role to reliably estimate the extent with which *CRR* varies in soil deposits. Surface wave measurements, for example, can rapidly characterize V_S spatial variability. However, they suffer from analytical limitations related to the wavefield transforms typically used to process the signals into a dispersion curve. Additionally, the forward modeling used to compute theoretical dispersion curves during inversion assumes uniform, contiguous strata throughout the site. Any lateral variations in subsurface stiffness are subsequently ignored. Consequently, the waveform measurements from a linear receiver array result in a 1D V_S profile assumed on average to represent the conditions beneath the array center.

The goal of this study was to explore advanced methodologies by which to process surface waves and recover spatial variability of natural soil deposits. More specifically, numerical modeling was performed to compare V_S estimates from full waveform inversion (FWI) of surface waves to the typical dispersion-based approach. FWI attempts to directly match the raw signals to synthetic signals from numerical modeling. Only a limited number of recent studies have examined FWI at the geotechnical scales of interest (e.g., Fathi et al. 2016). In this study, FWI was performed for a stochastic RFM generated with a spatially-correlated Gaussian random V_S distribution. The resulting V_S estimates were compared to those from simulated two-dimensional (2D) MASW testing. Predictions for the *FS* against liquefaction triggering were made using the V_S-*CRR* correlations recommended by Kayen et al. (2013) and subsequently compared.

2 EXPERIMENTAL EFFORTS

2.1 *Model domain*

The domain for this study was developed using a stochastic model with spatially-correlated V_S values (Fig. 1). The MATLAB® script used to define this model applies a Gaussian correlation function to generate the random V_S field through lower-upper (LU) decomposition of the covariance matrix. The domain consists of a single 10.0 m deep layer of alluvial soil that extends 80.0 m in length and has an average V_S = 200 m/s. The domain was generated with a 0.5 m mesh size in both the horizontal and vertical direction. The ground water table was located at z =1.0 m.

The MATLAB® script was then used to generate a random V_S field that mimics the spatial stiffness variability found in natural soil deposits. The coefficient of variation (COV) for V_S was set to 30%, which compares with coarse-grained alluvial soils (e.g., Phoon & Kulhawy 1999). The spatial extent of variability along the vertical and horizontal directions was set to θ_z = 0.5 m and θ_x = 10.0 m, which is consistent with other studies (e.g., Montgomery & Boulanger 2016) and with the observation that θ_x is typically at least an order of magnitude larger than θ_z (Phoon & Kulhawy 1999). In the zone above the water table, the soil P-wave velocities (V_P) were derived from V_S:

$$\frac{V_P^2}{V_S^2} = \frac{2(1-v)}{(1-2v)} \tag{3}$$

where the Poisson's ration (v) was set to 0.2. However, once below the water table, V_P in soils does not vary significantly from the V_P of water (approximately 1500 m/s). So V_P was fixed in the model as 1500 m/s below z = 1.0 m. The mass density (ρ) of the soil was estimated from V_S:

$$\rho = 0.277 + 0.648 \log V_S \tag{4}$$

where V_S is input in m/s and ρ is in g/cm^3 (Burns & Mayne, 1996).

Once the RFM was generated, the V_S and ρ values were used to estimate the depth-dependent *CSR* and *CRR* using the relationships recommended by Kayen et al. (2013). Based on the

water table location and the ρ of the soil, σ'_{vo} and σ_{vo} were computed for use in Equation 2. The MSF and r_d relationships proposed by Kayen et al. (2013) were also used in Equation 2:

$$r_d = \frac{\left(1 - \frac{-23.013 - 2.949 \cdot PGA + 0.999 \cdot M + 0.0525 \cdot V^*_{S,12m}}{16.258 + 0.201 \cdot exp\left[0.341 \cdot \left(-d + 0.0785 \cdot V^*_{S,12m} + 7.586\right)\right]}\right)}{\left(1 - \frac{-23.013 - 2.949 \cdot PGA + 0.999 \cdot M + 0.0525 \cdot V^*_{S,12m}}{16.258 + 0.201 \cdot exp\left[0.341 \cdot \left(0.0785 \cdot V^*_{S,12m} + 7.586\right)\right]}\right)} \tag{5}$$

$$MSF = 15 \cdot M^{-1.342} \tag{6}$$

where $V^*_{S,12m}$ represents the average V_S in the upper 12 m (i.e., 200 m/s). A PGA of 0.3g was used for a M = 7.5 event in the computation of CSR. CRR was computed using the Kayen et al. (2013) probabilistic framework:

$$CRR = exp\left\{\frac{\left[(0.0073 \cdot V_{S1})^{2.8011} - 2.6168 \cdot \mathrm{In}M - 0.0099 \cdot \mathrm{In}\sigma'_{vo} + 0.0028 \cdot FC - 0.4809 \cdot \Phi^{-1}(P_L)\right]}{1.946}\right\} \tag{7}$$

where Φ^{-1} is the complementary cumulative distribution function for a probability of liquefaction (P_L), FC is the fines content correction factor, and V_{S1} is the normalized V_S:

$$V_{S1} = C_{Vs} \cdot V_S = \left(\frac{P_a}{\sigma'_{vo}}\right)^{0.25} \cdot V_S \tag{8}$$

where C_{VS} is the overburden correction factor (≤ 1.5) and P_a is a reference stress of 1 atm. For a deterministic evaluation of liquefaction triggering, Kayen et al. (2013) recommend using P_L = 15% in Equation 7 and a FS = 1.17. Figure 1 presents the calculated CSR, CRR, and FS against liquefaction triggering for the model domain.

2.2 *Forward modeling and inversion*

The propagation of seismic waves was modeled with SPECFEM2D (Tromp et al. 2008). SPECFEM2D uses the Spectral Element Method (SEM), which formulates the wave equations using

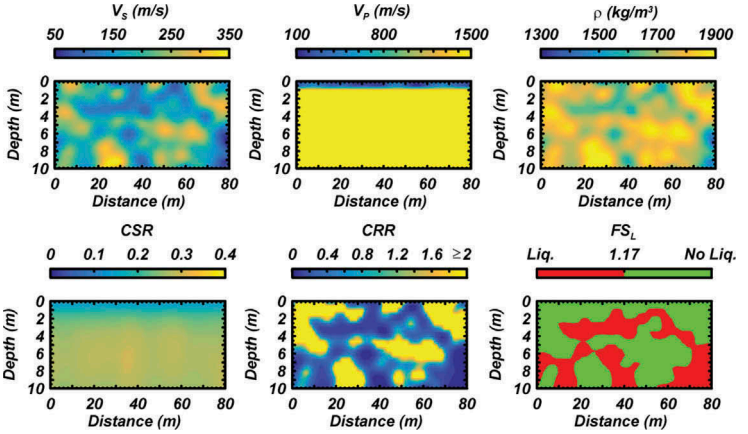

Figure 1. Model domain: V_S, V_P, ρ, CSR, CRR, and FS_L.

the same weak implementation in the Finite Element Method (FEM) but with higher degree piecewise polynomial basis functions. The higher order basis functions combined with the nodal interpolation scheme generates a diagonal mass matrix, which simplifies matrix inversion.

The spatially variable V_S, V_P, and ρ RFM defined the domain in SPECFEM2D. Forward modeling of wave propagation proceeded with a stress-free top surface and Stacey absorbing boundaries along the other domain limits. The stress-free boundary modeled the free surface and allowed the development of surface waves as solutions to the wave equations. The Stacey absorbing boundaries prevented reflections from the bottom and sides of the model.

Forward modeling was used to generate "observed" waveforms. For 2D MASW, receivers were placed along the ground to mimic 48 channel linear arrays with a 0.5 m interval (dx) and total array length of 23.5 m. The first array channel was located at 10.5 m and its last channel was at 34.0 m. The input signal was a 30 Hz Ricker wavelet located at a source offset (SO) of 10.0 m from the first channel (i.e., $SO = 20dx$). The subsequent waveforms were processed using the Geometrics SeisImager/SW® software. A fundamental-mode dispersion curve was extracted and inversion was performed using a local search algorithm. SeisImager/SW® estimates the initial V_S model by plotting the dispersion curve phase velocities at one-third the corresponding wavelength. V_P was fixed at 1500 m/s during inversion to mimic the shallow water table. The misfit between observed and theoretical dispersion curves was minimized to within a root-mean-square error (RMSE) of 5% using a non-linear least squares approach. V_S was subsequently plotted at the midpoint of the array. Data processing was repeated after the array and source were each shifted by 0.5 m until the edge of the domain was reached at 79.5 m. This resulted in 92 one-dimensional (1D) V_S profiles that were then linearly interpolated to create a 2D V_S profile. Linear interpolation was performed to smooth the resulting step-wise V_S depth profile.

FWI was performed using the open source inversion software code SeisFlows (Mordak et al. 2018) with SPECFEM2D as the forward modeler. The initial starting model consisted of a uniform layer with V_S = 200 m/s and V_P = 1500 m/s. Many of the same parameters for 2D MASW forward modeling (e.g., mesh and time step) were used for FWI. However, optimal data acquisition parameters differ between a dispersion-based inversion approach and FWI. So the spatial extent of source and receiver locations was modified for FWI relative to 2D MASW. The inversion process was performed with the waveforms recorded by all receiver locations across the model (i.e., 80 receivers spaced 1.0 m apart from x = 0.5 m to x = 79.5 m). Ricker wavelet sources (10 Hz, 20 Hz, and 30 Hz) were located from 1.0 m to 79.0 m at 1.0 m spacing. Masking was used to prevent V_S updates in the upper 1.0 m since the soil above the ground water table was unlikely to liquefy. This improved inversion stability because the large misfit gradients typically adjacent to source and receivers were ignored. Relative misfit between the "observed" and forward modeling waveforms was computed using the L_2-norm (i.e., Euclidian norm). FWI was completed when this relative misfit decreased to approximately 5%.

3 RESULTS AND ANALYSIS

3.1 *Dispersion-based approach*

The 2D MASW V_S profile is presented in Figure 2 along with the subsequent estimates for V_P, ρ, CSR, CRR, and FS_L based on Equations 1 – 8. Spatial coverage is limited from x = 22.25 m to 67.75 m with V_S estimates missing from approximately 35.0 m of the domain. This resulted from locating the 1D V_S profiles at the centers of their respective linear arrays. Complete coverage during field testing would therefore require additional measurements with the array located at least partially outside the boundaries of the test site. Site constraints may render this impractical and costly both in terms of expenses and data acquisition efforts.

Generally, the 2D MASW results did capture some of the variability present in the domain. For example, the V_S values corroborated the presence of a stiffer zone near the bottom of the domain between x = 20.0 m to 30.0 m. However, V_S principally showed evidence of softer conditions relative to the true model. For example, approximately 50% of the true model exhibits V_S above the average value of 200 m/s in the zone sampled by 2D MASW. However, this percentage drops to approximately 15% in the profiles presented in Figure 2. When the 2D MASW V_S

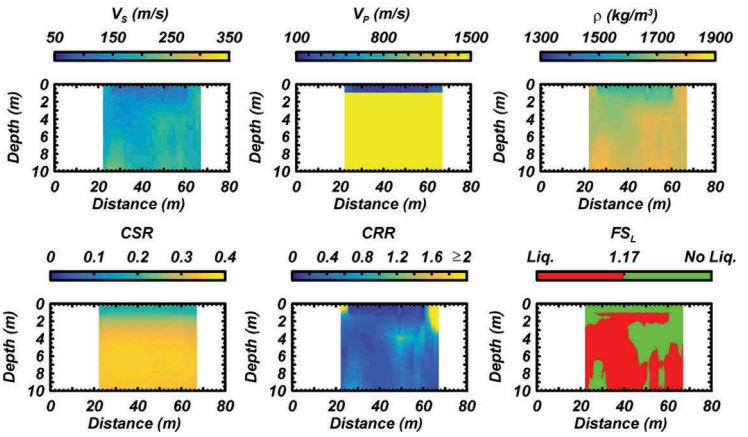

Figure 2. Dispersion-based MASW results: V_S, V_P, ρ, CSR, CRR, and FS_L.

at a given depth and location was compared to the true model V_S, the 2D MASW results underestimated V_S over approximately 67% of the sampled domain. This can be attributed to the spatial "averaging" introduced by the data acquisition process and wavefield transformation.

Another issue was the complexity of interpreting the fundamental-mode dispersion curve. In multiple locations, the subsurface exhibited a velocity reversal that trapped a low velocity layer beneath two stiffer layers. This increased participation from higher modes and sometimes obscured the fundamental mode. This was particularly the case near the end of the domain (x = 60.0 m – 68.0 m) where stiffer zones were located immediately below the surface. Given the presence of appreciable spatial variability in natural soil deposits, a dispersion-based approach may need to resort to multi-modal inversion when predicting liquefaction triggering.

3.2 *Full Waveform Inversion*

Figure 3 presents the FWI results. These results more thoroughly covered the spatial extent of the model domain. Additionally, FWI more accurately estimated V_S values. For example, the stiffer zone near the bottom of the domain between x = 20.0 m to 30.0 m is again visible in Figure 3. But there are also V_S values larger than 250 m/s highlighting the stiffer zones between x = 50.0 m – 65.0 m (at z = 4.0 m – 9.0 m) and x = 70.0+ m (z = 2.0 m). FWI V_S results were generally within ±10% of the true model V_S over approximately 25% of the entire domain. Focusing on the zone covered by 2D MASW, this percentage drops to 14% for the V_S results using a dispersion-based analysis. The results from FWI didn't also seem to be biased towards one range of V_S estimates as was the case with 2D MASW that tended to spatially average towards smaller V_S values. For example, FWI V_S results were just as likely to overestimate (44%) as they were to underestimate (55%) the true model V_S. Where the FWI results started to suffer was in the immediate vicinity of the two corners of the model where there is not enough spatial distribution of data to inform the inversion process.

3.3 *Discussion*

Given that the goal of a liquefaction triggering analysis is to establish the *FS*, it is useful to examine how both surface wave approaches performed relative to the true model. Figure 4 presents the *FS* estimated from the MASW and FWI V_S values. These results are overlain on top of the *FS* depth profile generated by the true model parameters.

Immediately apparent in Figure 4 is the conservative nature of the MASW results relative to FWI. Since 2D MASW exhibited more spatial averaging, the lower V_S values reduced *CRR* relative to the true model and FWI results. This resulted in predictions for liquefaction triggering over a much larger area. In fact, 2D MASW predicted that liquefaction could be triggered in nearly 60% of the sampled domain for the 0.3*g* PGA in this study. The actual triggered percentage in this measurement zone was only 39% based on the true model *FS*.

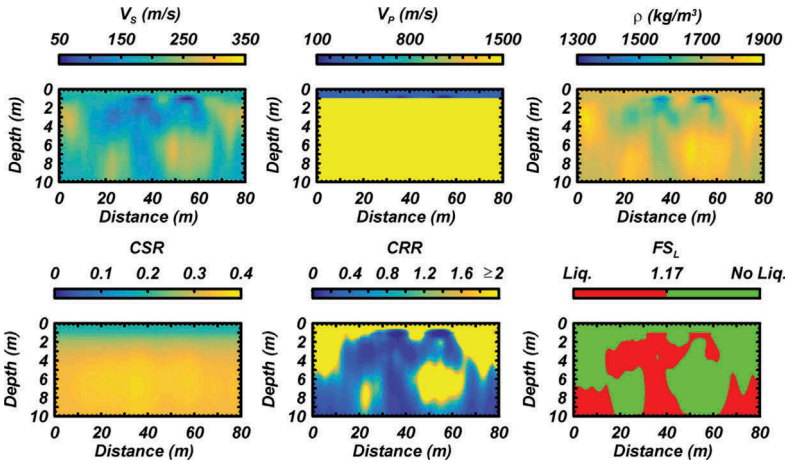

Figure 3. FWI results: V_S, V_P, ρ, CSR, CRR, and FS_L.

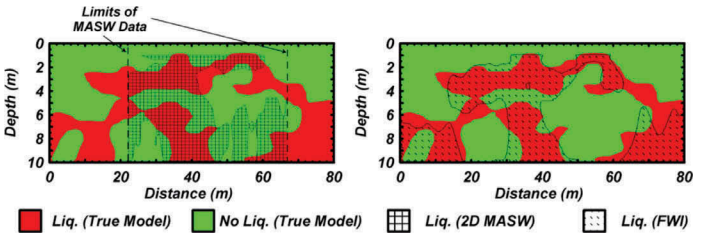

Figure 4. Comparisons of FS_L using dispersion-based MASW and FWI.

The FWI *FS* predictions, on the other hand, were more consistent with those derived from the real soil properties of the model domain. The total area expected to liquefy was 37% based on the FWI results, which agreed well with the 39% across the entire model. Based purely on volume of material expected to liquefy, the FWI results would seemingly predict similar levels of volumetric strain to the true model. However, despite this good agreement, an examination of Figure 4 highlights that the FWI results still misclassified potentially liquefiable or non-liquefiable zones. For example, the FWI results failed to connect the zone between approximately x = 60.0 m – 70.0 m and z = 3.0 m – 5.0 m. The FWI also fused together the upper liquefiable crust and the lower bulb present at the bottom of the domain at approximately x = 40.0 m. In fact, the FWI results only accurately matched with 68% of the zone predicted to liquefy based on the true model properties (i.e., the hatched zone only matches up with the red zone 68% of the time). Nevertheless, these results were still superior to the 2D MASW results for *FS*.

4 CONCLUSIONS

The results from this study highlighted the potential superiority of FWI when evaluating spatial variability of liquefaction triggering for natural soil deposits. The FWI V_S profile was more accurate, exhibited similar variability, and was less biased by spatial averaging when compared to the MASW results. More accurate FWI V_S estimates led to better agreement with the true model liquefaction *FS*. However, FWI was only able to correctly identify liquefaction triggering within 68% of the zone predicted from true model properties. Nevertheless, the overall area expected to liquefy was similar, which signifies that predicted post-liquefaction settlements would likely be similar as well. 2D MASW was shown to systematically underestimate V_S and predict excessively conservative *FS*. However, it should be noted that 2D MASW is a more established technique with wider adoption and fewer issues related to

field implementation. Noisy data, source uncertainty, and three-dimensional (3D) effects complicate field-based FWI relative to the idealized conditions presented in this numerical study. Nevertheless, surface wave testing using dispersion-based inversion or FWI would likely improve site characterization for liquefaction triggering analysis relative to point-based SPT and CPT methodologies.

ACKNOWLEDGEMENTS

This research includes calculations carried out on Temple University's HPC resources and thus was supported in part by the National Science Foundation through major research instrumentation grant number 1625061 and by the US Army Research Laboratory under contract number W911NF-16-2-0189.

REFERENCES

Andrus, R.D., & Stokoe II, K.H. 2000. Liquefaction resistance of soils from shear-wave velocity. *J. of Geotech. Geoenviron. Eng*. 126(11):1015–1025.

Baker, J.W., & Faber, M.H. 2008. Liquefaction risk assessment using geostatistics to account for soil spatial variability. *J. Geotech. Geoenviron. Eng*. 10.1061/(ASCE)1090-0241(2008)134:1 (14):14–23.

Ben Salem, Z., Frikha, W., & Bouassida, M. (2017). Effects of Densification and Stiffening on Liquefaction Risk of Reinforced Soil by Stone Columns. *J. Geotech. Geoenviron. Eng*. 143(10), 06017014.

Bong, T., & Stuedlein, A.W. 2017. Spatial Variability of CPT Parameters and Silty Fines in Liquefiable Beach Sands. J. Geotech. Geoenviron. Eng. 143(12):04017093.

Boulanger, R.W., & Idriss, I.M. 2014. *CPT and SPT based liquefaction triggering procedures*. Report No. UCD/CGM-14/01. Center for Geotechnical Modeling, University of California, Davis. 134 pp.

Burns, S.E., & Mayne, P.W. 1996. Small- and high-strain measurements of in situ soil properties using the seismic cone penetrometer. *Transp. Res. Rec*. 1548:81-88.

Chung, J., & Rogers, J.D. 2017. Deterministic and Probabilistic Assessment of Liquefaction Hazards Using the Liquefaction Potential Index and Liquefaction Reduction Number. *J. Geotech. Geoenviron. Eng*. 143(10):04017073.

Fathi, A., Poursartip, B., Stokoe, II, K.H., & Kallivokas, L.F. 2016. Three-dimensional P- and S-wave velocity profiling of geotechnical sites using full-waveform inversion driven by field data. *Soil Dyn. Earthq. Eng*. 87:63-81.

Kayen, R.R., Moss, R.E.S., Thompson, E.R., Seed, R.B., Cetin, K.O., Derkiureghian, A., Tanaka, Y., & Tokimatsu, K. 2013. Shear wave velocity-based probabilistic and deterministic assessment of seismic soil liquefaction potential. *J. Geotech. Geoenviron. Eng*. 139(3):407–419.

Modrak, R.T., Borisov, D., Lefebvre, M., & Tromp, J. 2018. SeisFlows—Flexible waveform inversion software. *Comp. Geosci*. 115:88-95.

Montgomery, J., & Boulanger, R.W. 2016. Effects of spatial variability on liquefaction-induced settlement and lateral spreading. *J. Geotech. Geoenviron. Eng*. 143(1): 04016086.

National Academies of Sciences, Engineering, & Medicine (NASEM). 2016. *State of the Art and Practice in the Assessment of Earthquake-Induced Soil Liquefaction and Its Consequences*. Washington, DC: The National Academies Press. doi: 1017226/23474

Phoon, K.K., & Kulhawy, F.H. 1999. Characterization of geotechnical variability. *Can. Geotech. J*. 36 (4): 612–624.

Popescu, R., Prevost, J.H., & Deodatis, G. 2005. 3D effects in seismic liquefaction of stochastically variable soil deposits. *Geotechnique* 55(1):21–31.

Robertson, P.K., & Wride, C.E. 1998. Evaluating cyclic liquefaction potential using the cone penetration test. *Can. Geotech. J*. 35(3):442–459.

Seed, H.B., & Idriss, I.M. 1971. Simplified procedure for evaluating soil liquefaction potential. *J. of Geotech. Eng. Div*. 97(9):1249–1273.

Seed, H.B., Tokimatsu, K., Harder Jr., L.F., & Chung, R. 1985. Influence of SPT procedures in soil liquefaction resistance evaluations. *J. of Geotech. Eng*. 111(12):1425–1445.

Tromp, J., Komatitsch, D., & Liu, Q. 2008. Spectral-element and adjoint methods in seismology. *Comm. Comp. Phys*. 3(1):1–32.

Turner, B. J., Brandenberg, S. J., & Stewart, J. P. 2016. Case study of parallel bridges affected by liquefaction and lateral spreading. *J. Geotech. Geoenviron. Eng*. 142(7):05016001.